Free energy analysis of conductivity and charge selectivity of M2GlyR-derived synthetic channels

Jianhan Chen and John M. Tomich

Published Version Information

Citation: Chen, J., & Tomich, J. M. (2014). Free energy analysis of conductivity and charge selectivity of M2GlyR-derived synthetic channels. Biochimica et Biophysica Acta – Biomembranes, 1838(9), 2319-2325.

Digital Object Identifier (DOI): doi:10.1016/j.bbamem.2014.02.016

Publisher's Link: http://www.sciencedirect.com/science/article/pii/S0005273614000807

Free Energy Analysis of Conductivity and Charge Selectivity of M2GlyR-Derived Synthetic Channels

Jianhan Chen* and John M. Tomich*

Department of Biochemistry and Molecular Biophysics

Kansas State University

Manhattan, KS 66506, USA

Submitted to *BBA-Biomembranes* as a *Regular Paper*

Special Issue on "Interfacially active peptides and proteins"

Corresponding Authors: Phone: (785) 532-2518 (JC), (785) 532-6297 (JT); Fax: (785) 532-7278; Email: jianhanc@ksu.edu (JC), jtomich@ksu.edu (JT);

Abstract

Significant progresses have been made in the design, synthesis, modeling and *in vitro* testing of channel-forming peptides derived from the second transmembrane domain of the α-subunit of the glycine receptor (GlyR). The latest designs, including p22 (KKKKP ARVGL GITTV LTMTT QS), are highly soluble in water with minimal aggregation propensity and insert efficiently into cell membranes to form highly conductive ion channels. The last obstacle to a potential lead sequence for channel replacement treatment of CF patients is achieving adequate chloride selectivity. We have performed free energy simulation to analyze the conductance and charge selectivity of M2GlyR-derived synthetic channels. The results reveal that the pentameric p22 pore is non-selective. Moderate barriers for permeation of both K^+ and Cl^- are dominated by the desolvation cost. Despite previous evidence suggesting a potential role of threonine side chains in anion selectivity, the hydroxyl group is not a good surrogate of water for coordinating these ions. We have also tested initial ideas of introducing additional rings of positive changes to various positions along the pore to increase anion selectivity. The results support the feasibility of achieving anion selectivity by modifying the electrostatic properties of the pore, but at the same time suggest that the peptide assembly and pore topology may also be dramatically modified, which could abolish the effects of modified electrostatics on anion selectivity. This was confirmed by subsequent two-electrode voltage clamp measurements showing that none of the tested mono-, di- and tri-Dap substituted sequences was selective. The current study thus highlights the importance of controlling channel topology besides modifying pore electrostatics for achieving anion selectivity. Several strategies are now being explored in our continued efforts to design an anion selective peptide channel with suitable biophysical, physiological and pharmacological properties as a potential treatment modality for channel replacement therapy.

Keywords: cystic fibrosis; molecular dynamics; potential of mean force; anion selectivity; ion channels; peptide design

1. Introduction

Ion channels regulate the movement of charged species through cellular membranes and play central roles in communication between a cell and its environment [1, 2]. Defective ion channels are frequently implicated in human diseases including diabetes, cystic fibrosis (CF) and Alzheimer's dementia [3-5]. For example, mutations in the cystic fibrosis transmembrane conductance regulator (CFTR) protein lead to impaired channel activity and abnormal epithelial electrolyte transport, which in turn result in accumulation of mucus that underlies the key clinical manifestations of CF such as airway inflammation and bacterial infection [6]. Synthetic channel-forming peptides, especially those derived from transmembrane (TM) segments of biological channel proteins, have provided excellent models for understanding ion channel structure and function with small system sizes and more accessible biophysical properties [7-10]. These synthetic peptide channels also provide a promising option for channel replacement treatment of diseases caused by defective channel proteins [11-13]. A particularly desirable strategy is to deliver a soluble surface-active peptide to the apical surface of effected epithelia, which then spontaneously inserts into the cell membrane and forms ion-conducting pores. For this, an optimal peptide sequence should be highly soluble in aqueous solution with minimal aggregation tendency. Specifically for restoring chloride conductance for CF patients, the synthetic peptide channel needs to provide high anion conduction rates together with adequate chloride selectivity.

Previous studies showed that the second TM domain of the α_1–subunit of the glycine receptor (M2GlyR: P ARVGL GITTV LTMTT QSSGS RA) could self assemble to form homo anion-selective channels in phospholipid bilayers and cellular membranes [8, 9]. Numerous modifications have since been made to the original 23-amino acid sequence to increase aqueous solubility, suppress aggregation propensity, and enhance insertion efficiency and ion conductance [13-20]. Interestingly, these M2GlyR-derived peptides do not appear to trigger immune or inflammatory responses at clinically relevant doses [21]. A leading candidate for replacing CFTR channels identified through these studies is p22 (KKKKP ARVGL GITTV LTMTT QS). The poly-lysine N-terminus increases the aqueous solubility ~10-fold and also ensures the uniformity of membrane insertion (C-terminus first) [13]. Truncation of the five C-terminal residues (SGSRA) significantly reduces peptide oligomerization and aggregation in the aqueous phase without compromising the channel activity compared to the full-length version

[16]. Replacement of Ser22 with a membrane anchoring tryptophan (p22-S22W) further suppresses non-productive aqueous solution assemblies and reduces the peptide concentration required for maximal channel activity. For example, p22-S22W requires only $K_{1/2} \sim 46$ μM to reach the one-half of the maximum short-circuit current I_{max} across Madin-Darby canine kidney (MDCK) epithelial monolayers, compared to that of $K_{1/2} \sim 210$ μM for p22. However, p22-S22W is about 50% less conductive than p22, reducing I_{max} from ~23.7 μA cm^{-2} to ~13.0 μA cm^{-2}. We have previously combined solution NMR and molecular modeling to construct atomistic structural models of the pentameric channels of p22 and p22-S22W [19] (also see Fig. 1). Atomistic molecular dynamics (MD) simulations in POPC bilayers suggest that the membrane-anchoring tryptophan residues not only rigidify the whole channel, suggesting increased stability, but also reduce the pore opening, consistent with lower measured conductance. The same structural model was later used to predict the pore structural features of another mutated sequence, p22-T19R,S22W, based on more extensive MD simulations up to 200 ns in length [20]. The results proved fully consistent with parallel NMR, cysteine scanning and other biophysical characterizations and further established that the pore most likely involved left-handed helix assembly similar to what was observed in all available crystal structures of cys-loop ligand-gated channels [22-24]. The success of simulation in recapitulating non-trivial functional differences between p22 and its amino acid replacement variants provides an important validation of the pentameric channel structural model.

One of the key remaining barriers to having a lead peptide for potential clinical testing for CFTR channel replacement therapy is a lack of sufficient anion selectivity. The original M2GlyR 23-residue peptide was estimated to be 85% anion selective based on single-channel currents measured in POPE/POPC membranes [9]. Replacement of both Arg residues in the original sequence with Glu converted the channel to be 84% cation selective [9], suggesting an essential role of electrostatics in determining charge selectivity. The C-terminal truncation introduced in p22 and its mutants is necessary to suppress oligomerization and lowers the active concentrations, but also removes the key C-terminal Arg responsible for anion selectivity. Early whole-cell patch clamp experiment using a human colonic carcinoma cell line (HT-29) indicated that p22 and p22-T19R, S22W should retain substantial anion permselectivity, albeit weaker compared to the original sequence [18]. However, experimental difficulties associated with spontaneous insertion of M2GlyR-derived peptides into artificial phospholipid bilayers have so

far prevented quantification of charge selectivity of the assembled pores (even though most M2GlyR-derived peptides do insert efficiently into cell membranes). In our previous simulations of the p22 and p22-S22W pentameric pores, we observed that Cl^- ions remain highly solvated and coordinated with pore-lining threonine side-chains (particularly Thr13 and Thr17) for substantial times (~ 1 ns) during spontaneous transport [19]. Previous studies have suggested that –OH group preferably stabilizes Cl^- with respect to Na^+ and K^+ [25-27], even though threonine side chains have received little attention as a possible contributing factor in anion selective protein channels. In this work, we preformed free energy simulations and analysis to test the hypothesis that rapid reversible binding of Cl^- to one or more threonine hydroxyls can contribute to anion selectivity of the p22 pore. We also performed computational mutagenesis and MD simulations as initial tests of several possible new designs that aim to modulate the electrostatic properties of the pore to achieve anion selectivity.

2. Materials and Methods

2.1. Umbrella sampling and analysis

Atomistic structural models of p22 and p22-S22W channels were previous constructed by combining information from solution NMR, biophysical data on the oligomeric state and pore-lining residues, and molecular modeling [28]. These models provided a structural basis for several key functional consequences of introducing a single C-terminal tryptophan, in particular, the observation that a significant increase in the apparent stability of the p22-S22W pore was accompanied with nearly 50% reduction in conductance. Umbrella sampling was used to calculate the potentials of mean force (PMFs) of Cl^- and K^+ permeation through the p22 channel model [29-31]. Harmonic restraint potentials were placed on a single selected Cl^- or K^+ ions, centered at every 1.0 Å along the membrane normal (z axis) with a force constant 5.0 kcal/mol/$Å^2$. A weak flat-bottom cylindrical restraint with an 8 Å radius was imposed on the selected ion to restrict lateral displacement outside of the pore [30, 31]. The initial conformations for all umbrella windows were generated using short steered molecular dynamics (MD) simulations initiated from the equilibrated channel model structure from our previous work [28]. The total number of windows was 61, covering z = -30 to 30 Å (with respect to the center of the mass of the pore). As illustrated in Fig. 1, each initial conformation contains 106 POPC lipids,

5367 waters, 40 Cl^- ions and 10 K^+ ions in a rectangular box of ~66 × 66 × 71 $Å^3$. The effective ion concentration is ~50 mM. All simulations were preformed using CHARMM [32, 33] in the param22 all-atom force field with CMAP [34-36]. SHAKE [37] was used to constrain the length of hydrogen-attaching bonds to allow for a 2 femtosecond dynamic time step. Particle Mesh Ewald (PME) [38] was used for treatment of long-range electrostatic interactions, and van der Waals interactions were smoothly switched off between 10 and 12 Å. Constant temperature and pressure (NPT) simulations were performed at 300 K and 1 atmospheric pressure. The length of sampling for each umbrella window was 1.0 ns, which has proven to be sufficient for achieving excellent convergence in previous PMF calculations of ion permeation through small channels [30, 31].

The single-ion PMF was first calculated from the umbrella sampling trajectories using WHAM [39]. The convergence was examined by comparing the results calculated from the second half and all data. The single-ion PMF calculated from umbrella sampling is only valid for pore regions with single-ion occupancy. The single-ion pore region was determined by analyzing the distributions of single and multiple-ion occupancy during the previous 20-ns equilibrium simulation [28]. The overall PMFs of ion permeation through the pore were constructed by blending the profiles derived from umbrella sampling and equilibrium simulation using linear interpolation [30, 31]. The conductance and charge selectivity were analyzed based on the overall PMFs of ion permeation. The diffusion constants of ions in bulk water were computed from the 20-ns equilibrium simulation trajectory. Coordinating waters and threonine hydroxyls for K^+ and Cl^- were identified as those with ion-oxygen distances no greater than 3.5 Å. The 3.5 Å cutoff distance was identified by examining the ion-water oxygen radial distribution functions, which approximately corresponds to the minimum between the first and second solvation peaks (data not shown).

2.2. MD simulations of mutated channels

Additional equilibrium simulations were performed to investigate the structural and functional consequences of introducing positive charged residues near the narrower C-terminal region of the pore. To facilitate later experimental testing, these mutations were introduced based on the more stable p22-S22W sequence. The first substituted sequence, p22-T19R, S22W, replaced the pore-lining Thr19 with Arg (referred to as p1130 hereafter). Three additional sequences were

investigated where smaller diaminopropionic acid (Dap) was introduced to the narrowest regions of the pore, at either Thr13 or Thr17 position, including p1130-T17Dap, p1130-T13Dap, T17Dap and p1130-T13Dap, T20Dap. The initial conformations for all four mutated pores were first built based the equilibrated p22-S22W pore structure from our previous work [28]. Multiple stages of energy minimization and restrained molecular dynamics were then performed to gradually equilibrated the pore structures, during which various restraints were applied to selected atoms and with gradually decreasing restraint strength [40]. Details of the equilibration protocol can be found in our previous work [28]. Once properly equilibrated, 20 ns NPT simulations were performed for each mutated pore in CHARMM, with the same setup as used in umbrella sampling (see above). The equilibrium simulations suggested that incorporation of rings of charges, especially the Dap mutants, significantly enhances spontaneous Cl^- permeation through the pore while maintaining large barriers for K^+ permeation. This allows well-converged free energy profiles of Cl^- permeation to be calculated directly from the equilibrium sampling for testing the effects of electrostatic mutations for enhancing charge selectivity. Therefore, more rigorous umbrella sampling was not performed.

3. Results and Discussion

3.1. PMFs of ion permeation

Fig. 2 examines the convergence of the single-ion PMFs calculated WHAM analysis of umbrella sampling simulations as well as the equilibrium PMFs derived directly from the 20-ns unbiased simulation. A first indication of the well-converged nature of the single-ion PMFs is minimal baseline distortion and assymetry (~0.3 kcal/mol) at large |z| values for K^+ permeation (green traces). For Cl^- permeation, the baseline appears distorted and assymetric at large positive z displacements (red traces). However, examination of the equilibrium PMFs (Fig. 2B) shows that there is a broad basin for Cl^- due to the oligo-lysine N-terminal tails. Convergence of the PMFs was further examined by comparing results calculated from all and only the second half of the 1.0 ns sampling. The results show that the maximum errors are ~1.0 kcal/mol and ~0.9 kcal/mol for K^+ and Cl^- PMFs, respectively. The average deviations between 0.5 and 1 ns PMFs are only 0.29 kcal/mol and 0.24 kcal/mol for K^+ and Cl^- PMFs, respectively. The equilibrium PMFs are also very well converged outside the pore (|z| > 20 Å; see Fig. 2B)

The single-ion PMFs calcuated using the umbrella sampling protocol (see Methods) are only valid in the pore region that is almost exclusively occupied by a single ion [30, 31]. To identify the single-ion region, we calculated the probilities of finding one or more ions within the 8 Å-radius cylinder centered at the pore center of mass as a function of z displacement. The results, shown in Fig. 3, reveal that the probility of finding two or more K^+ is minimal throughout the box (due to much lower effective K^+ concentration). This is consistent with the observation that the profiles of single-ion and equilibrium PMFs (Fig. 2 A and B) for K^+ permeation match well, except in high free energy regions with diminishing ion densities sampled during the unbiased simulation ($|z| < 16$ Å). However, there are significant probabilities of double and triple Cl^- occupancies near the C-terminal entrance of the pore, due to the presence of positively charged oligo-lysine tails (green and blue traces in Fig. 3). As a result, the single-ion PMF for Cl^- permeation deviates significantly from the correct PMF derived directly from the bulk ion densities sampled during the unbiased simulation.

The overall PMFs of ion permeation were constructed by blending the single-ion and equilibrium PMFs using linear interpolation [31]. Specifically, single-ion PMFs were used for the single occupancy regions of the pore (-17 to 7 Å for Cl^- and -17 to 25 Å for K^+). Note that the range for K^+ was chosen to best match the overlapping regions of the single-ion and equilibrium PMFs. The PMFs linearly switch to the equilibrium profiles within 2 Å outside of the chosen single occupancy ranges. As shown in Fig. 4, the locations of the major free energy barriers for both K^+ and Cl^- permeation coincide well with the pore opening profile. Comparing the overall PMFs of K^+ and Cl^- permeation, the main difference is the broad free energy basin near the C-terminal entrance of the pore (around $z = 10$ Å). Another key difference is that K^+ experiences a slightly broader but lower free energy barriers through the pore, while Cl^- permeation is subject to narrower but steeper barriers. The steeper barrier of Cl^- permeation can be apparently contributed to the large size. The most important observation, however, is that the pore lining threonine side chains do not appear to contribute to preferential stabilization of Cl^- during permeation, at least not to a level sufficient to lead to lower permeation free energy barrier. Fig. 5 analyzes how ions are dehydrated and coordinated by threonine side chains during permeation. This bulk hydration number, ~6.5, agree well with previous simulations of bulk 1 M KCl in TIP3P water [41]. Both K^+ and Cl^- remain highly solvated during permeation, losing no more than two coordinating waters even at the narrowest regions of the pore ($z \sim -10$ Å). Interestingly, despite the

observation of Cl^- pausing for ~1 ns near pore-lining threonines during spontaneous transport [19], the hydroxyl side chains do not appear to be a good surrogate of water for coordinating either K^+ or Cl^-. The average hydroxyl coordination number is no more than one even at the narrowest portion of the pore for both ions, which does not fully compensate for a loss of ~2 hydration waters. Partial desolvation seems to be main source of free energy barriers.

3.2. Maximum conductance and charge selectivity

Similar free energy barriers of modest heights observed in the overall PMFs for both K^+ and Cl^- suggest that the p22 pore is unlikely to be anion selective. To further quantify the charge selectivity of the pore, we estimated the maximum K^+ and Cl^- conductance based on the one-dimensional PMFs, $W(z)$, [42],

$$g_{\max} = \frac{e^2}{kTL^2}\left(L^{-1}\int_P D^{-1}(z)e^{W(z)/kT}\right)^{-1}\left(L^{-1}\int_P e^{-W(z)/kT}\right)^{-1}, \quad (1)$$

where e is unit electron charge, k is the Boltzmann constant, T is the temperature, $D(z)$ is the diffusion constant, and L is the length of the pore region. Eqn. 1 is valid under symmetric concentration baths and low membrane potential, and has been shown to provides a reasonable order-of-magnitude estimate of the maximum conductance under these conditions [43]. Mean square displacement analysis showed that the diffusion constants were ~1.54 nm^2/ns for chloride ions and ~2.09 nm^2/ns for potassium ions in TIP3P water. The diffusion constants in the pore region requires separation of the local dissipative forces that underlies diffusional motion of the ions from the average systematic forces arising from the PMF and harmonic restraint potentials. It has been previously determined that $D(z)$ is about 2/3 of bulk values within a narrow gramicidin channel [31]. The same 2/3 scaling down of bulk diffusion constants was used in the current estimation of maximum conductance. Taken the pore region to span $|z| < 18$ Å, the conductance was estimated to be ~5.2 pS for chloride ions and ~15 pS for potassium ions. The estimations are generally consistent with the range of 20-50 pS derived from single-channel recordings of related M2GlyR pores [9, 18]. The maximum conductance estimation further supports that the p22 pentameric pore likely has minimal anion permeation selectivity, despite existing evidences suggesting a plausible role of threonine rings in anion selectivity [25-27]. That is, removal of a key C-terminal arginine during the C-terminal truncation introduced to suppress peptide oligomerization and aggregation in the aqueous phase also abolishes the modest

residual anion selectivity present in the intact second TM domain of Gly. Mutagenesis studies of the intact GlyR α_1 channel further suggests a key role of maintaining a narrow pore besides electrostatics to support anion selectivity [44]. For example, deleting of the proline at the N-terminus of the second TM domain does not directly change the charge characteristics of the pore but reduces the anion selectivity (P_{Cl}:P_{Na}) from 27.9 to 3.8 [45], which has been attributed to an increase in the pore diameter from 5.4 Å to 6.9 Å. The N-terminal oligo-lysine tail introduced to improve the aqueous solubility also significantly expands the pore opening at the C-terminus (see Fig. 4A), which likely diminishes the electrostatic effects of the remaining N-terminal arginine (Arg7) on charge selectivity. Taken together, changes in both charge characteristics and pore profile likely explains a lack of anion selectivity predicted from the free energy analysis.

3.3. Charge mutations and anion selectivity

Previous free energy analysis of charge selectivity in Cys-Loop family channels has suggested that the overall electrostatics and presence of rings of charged residues near the pore entrance are likely sufficient to achieve charge electivity [27]. However, the free energy analysis shows that the oligo-lysine C-termini of the M2GlyR-derived pores doe not appear to be sufficient to achieve anion selectivity, mainly due to large opening at the N-terminal entrance of the pore. We have thus explored the idea of placing positive charges in the middle and narrow regions of the pore through computational mutagenesis. The sequence p1130 (p22-T19R, S22W) has been previously tested experimentally and shown to be more conductive and insert more efficiently into cell membrane compared to the parent p22-S22W sequence. Incorporation of additional natural lysine or arginine at other pore-lining positions (e.g., Thr13 and Thr17) leads to severe steric clash and does not appear feasible. Therefore, we investigated three additional sequences that incorporate smaller non-encoded 2,3-Diaminopropionic acid (Dap) residues at positions Thr13, Thr17 and/or Thr20, including p1130-T17Dap, p1130-T13Dap, T17Dap and p1130-T13Dap, T20Dap (see Methods). In the absence of any experimental knowledge on the possible topology and oligomeric states of these Dap-substituted pores, we only tested the structural and functional consequences of charge mutations in the context of the pentameric pore based on relatively short 20-ns equilibrium simulations. The results of these simulations are summarized in Fig. 6. Interestingly, all three pores (p1130-T17Dap, p1130-T13Dap, T17Dap and p1130-

T13Dap, T20Dap) appear to be stable throughout the simulation timespan, which is somewhat surprising considering exceedingly high charge density of the double Dap mutations. Nonetheless, electrostatic repulsion between positive charges dramatically affected the pore profiles. Introduction of a Dap substitution at position 17 opens up the C-terminal end, but the pore appears to be able to compensate by tighter packing of hydrophobic residues near position 10. With the double Dap substitutions, widening of the pore was observed throughout the pore. For all the Dap-substituted sequence, the occupancy of chloride ions in the pore is sufficiently high to allow direct calculation of the PMF from these equilibrium simulations. The results suggest that introduction of positively charged Dap substitutions could eliminate the free energy barriers of anion permeation, indicating that this may be an effective approach for achieving high anion conductance and selectivity simultaneously in M2GlyR-derived synthetic channels. Furthermore, the results also suggest that uniform placement of Dap substitutions such as at positions 13 and 20 might be optimal, providing smooth free energy profiles without strong traps or large barriers. On the other hand, the apparent (and surprising) stability of the charge mutants maybe misleading due to the limited timescale of the test simulations. Particularly pores with double Dap mutations appear to become so wide that the helix bundles are no longer tightly packed with few inter-peptide contacts. Previous experimental studies have demonstrated that M2GlyR-derived peptides likely form dynamic pores with heterogeneous oligomeric states [8, 9, 18]. Therefore, the pentameric assembly may no longer be the most stable form of the pore. If higher oligomeric states are more probable, the pore opening is expected be larger, which should reduce or even abolish the effectiveness of positively charge rings in providing anion selectivity.

In our most recent studies in Ussing Chambers using MDCK cells as well as single-channel recordings in Xenopus oocytes testing the Dap substituted sequences provided unexpected results [46]. All of the tested mono-, di- and tri-Dap substituted sequences induced short-circuit transepithelial currents when exposed to the apical membrane of MDCK cells. The sequences containing multiple Dap-substituted residues induced larger currents than peptides with single or no Dap-substitutions, consistent with the simulations showing that charge repulsion greatly increase the pore opening (Fig. 6). Employing two-electrode voltage clamp electrophysiology on oocytes treated with p22-T19R, S22W or the Dap-substitutions we observed that the Dap-substituted sequences induced significantly larger voltage-dependent currents than the parent compound, but with no apparent change in the reversal potentials upon replacement of the

external Na^+, Cl^- or K^+. These results indicate that the induced currents remained non-selective. Combined with the simulation results summarized in Fig. 6, the interpretation for lack of anion selectivity in these modified sequences is that introduction of additional rings of positive charges dramatically shift the oligomeric states of the peptide assembly in membrane and lead to much larger pores. Therefore, one needs to exploit strategies to control the peptide assembly besides electrostatics to actually achieve anion selectivity in M2GlyR-derived channels.

4. Conclusions

Significant progresses have been made in designing M2GlyR-derived channel-forming peptides with drastically improved biophysical properties and enhanced channel activities [18]. The last obstacle to a potential lead sequence for channel replacement treatment of CF patients is achieving adequate chloride selectivity. We have performed free energy simulation to analyze the conductance and charge selectivity of M2GlyR-derived synthetic channels. The results reveal that, despite previous evidence suggesting a potential role of threonine side chains in anion selectivity, the pentameric p22 pore is non-selective. Moderate barriers for permeation of both K^+ and Cl^- are dominated by the desolvation cost and the hydroxyl group is not a good surrogate of water for coordinating these ions. We have also tested initial ideas of introducing additional rings of positive changes to various positions along the pore to increase anion selectivity. The results support the feasibility of achieving anion selectivity by modifying the electrostatic properties of the pore, but at the same time suggest that the peptide assembly and pore topology may also be dramatically modified. Subsequent two-electrode voltage clamp measurements indicate that all tested mono-, di- and tri-Dap substituted sequences are much more conductive but none gives rise to anion selectivity. The implication is that introducing rings of positive charges do lead to higher oligomeric states and larger pores. The current study thus highlights the importance of controlling channel topology besides modifying pore electrostatics for achieving anion selectivity. For this, one may have to exploit earlier designs with longer sequences that form more tightly packed pores [16]. Alternatively, one may need to use scaffolds to restrict oligomer state of the assemble pore [9]. Future experiments are also planned in which the charge groups are staggered in the pore to create a cationic pathway without overly concentrating the cationic residues.

Acknowledgement

This work was supported by the National Science Foundation (MCB 0952514 to JC) and the National Institutes of Health (GM074096 to JT). Part of the computing for this project was performed on the Beocat Research Cluster at Kansas State University**,** which is funded in part by NSF grants CNS-1006860, EPS-1006860, and EPS-0919443. This work is contribution number 14-177-J from the Kansas Agricultural Experiment Station.

References

[1] P.C. Jordan, Fifty years of progress in ion channel research, IEEE Trans. Nanobioscience, 4 (2005) 3-9.

[2] B. Corry, S.H. Chung, Mechanisms of valence selectivity in biological ion channels, Cell. Mol. Life Sci., 63 (2006) 301-315.

[3] M.J. Welsh, A.E. Smith, Molecular mechanisms of CFTR chloride channel dysfunction in cystic-fibrosis, Cell, 73 (1993) 1251-1254.

[4] S.C. Cannon, Physiologic principles underlying ion channelopathies, Neurotherapeutics, 4 (2007) 174-183.

[5] J. Zhao, R. Hu, M.F. Sciacca, J.R. Brender, H. Chen, A. Ramamoorthy, J. Zheng, Non-selective ion channel activity of polymorphic human islet amyloid polypeptide (amylin) double channels, Phys. Chem. Chem. Phys., (2013).

[6] T.J. Jentsch, V. Stein, F. Weinreich, A.A. Zdebik, Molecular structure and physiological function of chloride channels, Physiol. Rev., 82 (2002) 503-568.

[7] S.H. White, W.C. Wimley, Membrane protein folding and stability: Physical principles, Annu. Rev. Biophys. Biomol. Struct., 28 (1999) 319-365.

[8] M. Oblatt-Montal, L.K. Buhler, T. Iwamoto, J.M. Tomich, M. Montal, Synthetic Peptides and 4-Helix Bundle Proteins as Model Systems for the Pore-Forming Structure of Channel Proteins .1. Transmembrane Segment M2 of the Nicotinic Cholinergic Receptor-Channel Is a Key Pore-Lining Structure, J. Biol. Chem., 268 (1993) 14601-14607.

[9] G.L. Reddy, T. Iwamoto, J.M. Tomich, M. Montal, Synthetic peptides and four-helix bundle proteins as model systems for the pore-forming structure of channel proteins. II. Transmembrane segment M2 of the brain glycine receptor is a plausible candidate for the pore-lining structure, J. Biol. Chem., 268 (1993) 14608-14615.

[10] S.K. Kandasamy, D.K. Lee, R.P. Nanga, J. Xu, J.S. Santos, R.G. Larson, A. Ramamoorthy, Solid-state NMR and molecular dynamics simulations reveal the oligomeric ion-channels of TM2-GABA(A) stabilized by intermolecular hydrogen bonding, Biochim. Biophys. Acta, 1788 (2009) 686-695.

[11] D.P. Wallace, J.M. Tomich, T. Iwamoto, K. Henderson, J.J. Grantham, L.P. Sullivan, A synthetic peptide derived from glycine-gated Cl- channel induces transepithelial Cl- and fluid secretion, American Journal of Physiology-Cell Physiology, 41 (1997) C1672-C1679.

[12] D.P. Wallace, J.M. Tomich, J.W. Eppler, T. Iwamoto, J.J. Grantham, L.P. Sullivan, A synthetic channel-forming peptide induces Cl- secretion: modulation by Ca2+-dependent K+ channels, Biochimica Et Biophysica Acta-Biomembranes, 1464 (2000) 69-82.

[13] J.M. Tomich, D. Wallace, K. Henderson, K.E. Mitchell, G. Radke, R. Brandt, C.A. Ambler, A.J. Scott, J. Grantham, L. Sullivan, T. Iwamoto, Aqueous solubilization of transmembrane peptide sequences with retention of membrane insertion and function, Biophys. J., 74 (1998) 256-267.

[14] J.R. Broughman, K.E. Mitchell, R.L. Sedlacek, T. Iwamoto, J.M. Tomich, B.D. Schultz, NH2-terminal modification of a channel-forming peptide increases capacity for epithelial anion secretion, American Journal of Physiology-Cell Physiology, 280 (2001) C451-C458.

[15] J.R. Broughman, L.P. Shank, O. Prakash, B.D. Schultz, T. Iwamoto, J.M. Tomich, K. Mitchell, Structural implications of placing cationic residues at either the NH2- or COOH-terminus in a pore-forming synthetic peptide, J. Membr. Biol., 190 (2002) 93-103.

[16] J.R. Broughman, L.P. Shank, W. Takeguchi, B.D. Schultz, T. Iwamoto, K.E. Mitchell, J.M. Tomich, Distinct structural elements that direct solution aggregation and membrane assembly in the channel-forming peptide M2GlyR, Biochemistry (Mosc.), 41 (2002) 7350-7358.

[17] J.R. Broughman, R.M. Brandt, C. Hastings, T. Iwamoto, J.M. Tomich, B.D. Schultz, Channel-forming peptide modulates transepithelial electrical conductance and solute permeability, American Journal of Physiology-Cell Physiology, 286 (2004) C1312-C1323.

[18] L.P. Shank, J.R. Broughman, W. Takeguchi, G. Cook, A.S. Robbins, L. Hahn, G. Radke, T. Iwamoto, B.D. Schultz, J.M. Tomich, Redesigning channel-forming peptides: Amino acid substitutions that enhance rates of supramolecular self-assembly and raise ion transport activity, Biophys. J., 90 (2006) 2138-2150.

[19] H.I. Herrera, A. Al-Rawi, G.A. Cook, J. Gao, T. Iwamoto, O. Prakash, J.M. Tomich, J. Chen, Structural Characterization of Two Channel-Forming Peptides: Consequences of Introduction a C-Terminal Tryptophan, Proteins: Struct., Funct., Genet., 78 (2010) 2238-2250.

[20] U. Bukovnik, J. Gao, G.A. Cook, L.P. Shank, M.B. Seabra, B.D. Schultz, T. Iwamoto, J. Chen, J.M. Tomich, Structural and biophysical properties of a synthetic channel-forming peptide: Designing a clinically relevant anion selective pore, Biochim. Biophys. Acta, 1818 (2012) 1039-1048.

[21] F.W. van Ginkel, T. Iwamoto, B.D. Schultz, J.M. Tomich, Immunity to a self-derived, channel-forming peptide in the respiratory tract, Clin. Vaccine Immunol., 15 (2008) 260-266.

[22] R.J.C. Hilf, R. Dutzler, X-ray structure of a prokaryotic pentameric ligand-gated ion channel, Nature, 452 (2008) 375-U312.

[23] N. Bocquet, H. Nury, M. Baaden, C. Le Poupon, J.P. Changeux, M. Delarue, P.J. Corringer, X-ray structure of a pentameric ligand-gated ion channel in an apparently open conformation, Nature, 457 (2009) 111-114.

[24] R.J.C. Hilf, R. Dutzler, Structure of a potentially open state of a proton-activated pentameric ligand-gated ion channel, Nature, 457 (2009) 115-U122.

[25] C. Emmeluth, B.L.J. Poad, C.D. Thompson, E.J. Bieske, Interactions between the chloride anion and aromatic molecules: Infrared spectra of the Cl--C6H5CH3, Cl--C6H5NH2 and Cl--C6H5OH complexes, J. Phys. Chem. A, 111 (2007) 7322-7328.

[26] S.O. Kang, R.A. Begum, K. Bowman-James, Amide-based ligands for anion coordination, Angewandte Chemie-International Edition, 45 (2006) 7882-7894.

[27] I. Ivanov, X.L. Cheng, S.M. Sine, J.A. McCammon, Barriers to ion translocation in cationic and anionic receptors from the Cys-loop family, J. Am. Chem. Soc., 129 (2007) 8217-8224.

[28] A.I. Herrera, A. Al-Rawi, G.A. Cook, J. Gao, T. Iwamoto, O. Prakash, J.M. Tomich, J. Chen, Structural characterization of two pore-forming peptides: consequences of introducing a C-terminal tryptophan, Proteins, 78 (2010) 2238-2250.

[29] G.M. Torrie, J.P. Valleau, Non-Physical Sampling Distributions in Monte-Carlo Free-Energy Estimation - Umbrella Sampling, J. Comput. Phys., 23 (1977) 187-199.

[30] T.W. Allen, O.S. Andersen, B. Roux, Molecular dynamics - potential of mean force calculations as a tool for understanding ion permeation and selectivity in narrow channels, Biophys. Chem., 124 (2006) 251-267.

[31] T.W. Allen, O.S. Andersen, B. Roux, Ion permeation through a narrow channel: Using gramicidin to ascertain all-atom molecular dynamics potential of mean force methodology and biomolecular force fields, Biophys. J., 90 (2006) 3447-3468.

[32] B.R. Brooks, R.E. Bruccoleri, B.D. Olafson, D.J. States, S. Swaminathan, M. Karplus, Charmm - a Program for Macromolecular Energy, Minimization, and Dynamics Calculations, J. Comput. Chem., 4 (1983) 187-217.

[33] B.R. Brooks, C.L. Brooks, A.D. Mackerell, L. Nilsson, R.J. Petrella, B. Roux, Y. Won, G. Archontis, C. Bartels, S. Boresch, A. Caflisch, L. Caves, Q. Cui, A.R. Dinner, M. Feig, S. Fischer, J. Gao, M. Hodoscek, W. Im, K. Kuczera, T. Lazaridis, J. Ma, V. Ovchinnikov, E. Paci, R.W. Pastor, C.B. Post, J.Z. Pu, M. Schaefer, B. Tidor, R.M. Venable, H.L. Woodcock, X. Wu, W. Yang, D.M. York, M. Karplus, CHARMM: The Biomolecular Simulation Program, J. Comput. Chem., 30 (2009) 1545-1614.

[34] A.D. MacKerell, D. Bashford, M. Bellott, R.L. Dunbrack, J.D. Evanseck, M.J. Field, S. Fischer, J. Gao, H. Guo, S. Ha, D. Joseph-McCarthy, L. Kuchnir, K. Kuczera, F.T.K. Lau, C. Mattos, S. Michnick, T. Ngo, D.T. Nguyen, B. Prodhom, W.E. Reiher, B. Roux, M. Schlenkrich, J.C. Smith, R. Stote, J. Straub, M. Watanabe, J. Wiorkiewicz-Kuczera, D. Yin, M. Karplus, All-atom empirical potential for molecular modeling and dynamics studies of proteins, J. Phys. Chem. B, 102 (1998) 3586-3616.

[35] A.D. Mackerell, M. Feig, C.L. Brooks, Extending the treatment of backbone energetics in protein force fields: Limitations of gas-phase quantum mechanics in reproducing protein conformational distributions in molecular dynamics simulations, J. Comput. Chem., 25 (2004) 1400-1415.

[36] A.D. MacKerell, M. Feig, C.L. Brooks, Improved treatment of the protein backbone in empirical force fields, J. Am. Chem. Soc., 126 (2004) 698-699.

[37] J.P. Ryckaert, G. Ciccotti, H.J.C. Berendsen, Numerical-Integration of Cartesian Equations of Motion of a System with Constraints - Molecular-Dynamics of N-Alkanes, J. Comput. Phys., 23 (1977) 327-341.

[38] T. Darden, D. York, L. Pedersen, Particle Mesh Ewald - an N.Log(N) Method for Ewald Sums in Large Systems, J. Chem. Phys., 98 (1993) 10089-10092.

[39] S. Kumar, D. Bouzida, R.H. Swendsen, P.A. Kollman, J.M. Rosenberg, The Weighted Histogram Analysis Method for Free-Energy Calculations on Biomolecules .1. the Method, J. Comput. Chem., 13 (1992) 1011-1021.

[40] S. Jo, T. Kim, W. Im, Automated Builder and Database of Protein/Membrane Complexes for Molecular Dynamics Simulations, PLoS One, 2 (2007) e880.

[41] W. Im, B. Roux, Ions and counterions in a biological channel: a molecular dynamics simulation of OmpF porin from Escherichia coli in an explicit membrane with 1 M KCl aqueous salt solution, J. Mol. Biol., 319 (2002) 1177-1197.

[42] B. Roux, M. Karplus, Ion-Transport in a Gramicidin-Like Channel - Dynamics and Mobility, J. Phys. Chem., 95 (1991) 4856-4868.

[43] B. Roux, Ion conduction and selectivity in K+ channels, Annu. Rev. Biophys. Biomol. Struct., 34 (2005) 153-171.

[44] M.L. Jensen, A. Schousboe, P.K. Ahring, Charge selectivity of the Cys-loop family of ligand-gated ion channels, J. Neurochem., 92 (2005) 217-225.

[45] A. Keramidas, A.J. Moorhouse, K.D. Pierce, P.R. Schofield, P.H. Barry, Cation-selective mutations in the M2 domain of the inhibitory glycine receptor channel reveal determinants of ion-charge selectivity, J. Gen. Physiol., 119 (2002) 393-410.

[46] U. Bukovnik, M. Sala-Rabanal, S. Francis, S.J. Frazier, B.D. Schultz, C.G. Nichols, J.M. Tomich, Effect of diaminopropionic acid (Dap) on the biophysical properties of a modified synthetic channel-forming peptide, Mol. Pharm., 10 (2013) 3959-3966.

[47] O.S. Smart, J.G. Neduvelil, X. Wang, B.A. Wallace, M.S.P. Sansom, HOLE: A program for the analysis of the pore dimensions of ion channel structural models, J. Mol. Graphics Modell., 14 (1996) 354-&.

Figures and Figure Legends

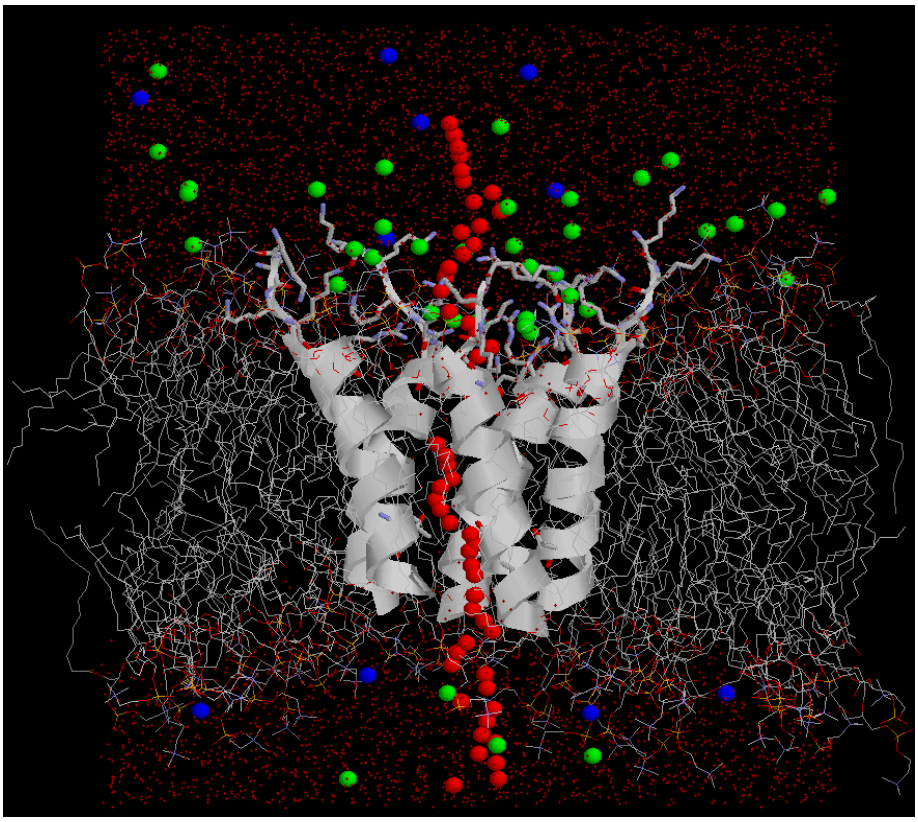

Figure 1. Initial conformations of umbrella sampling simulations. The pentameric p22 pore is represented using cartoon, with the oligo-lysine C-terminal tail shown in sticks. The POPC lipids are shown in thin sticks and only the oxygen atoms of water molecules are shown as red dots. Cl^- and K^+ ions are shown as green and blue spheres, respectively. The initial placements of a selected Cl^- for all 61 umbrella-sampling windows are overlaid on the initial conformation for the z = -30 Å window and then shown as red spheres.

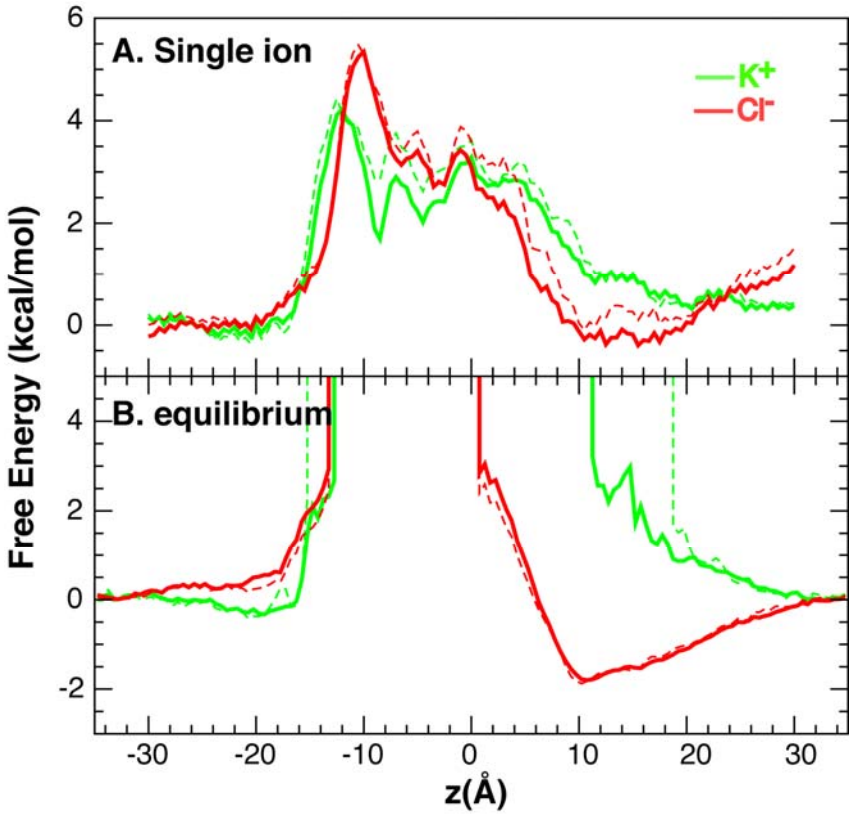

Figure 2. Free energy profiles as calculated from A) umbrella sampling and B) equilibrium simulations. The thick lines were computed using all data (1 ns per window in umbrella sampling and 20 ns in equilibrium simulation), and the thin dashed lines were computed using only the second half of the data. The equilibrium free energy profiles were converted from the probability distributions of finding either K^+ or Cl^- within the 8 Å-radius cylinder centered at the center of mass of the pore. *z* is the displacement from the center of the mass of the pore along the membrane normal.

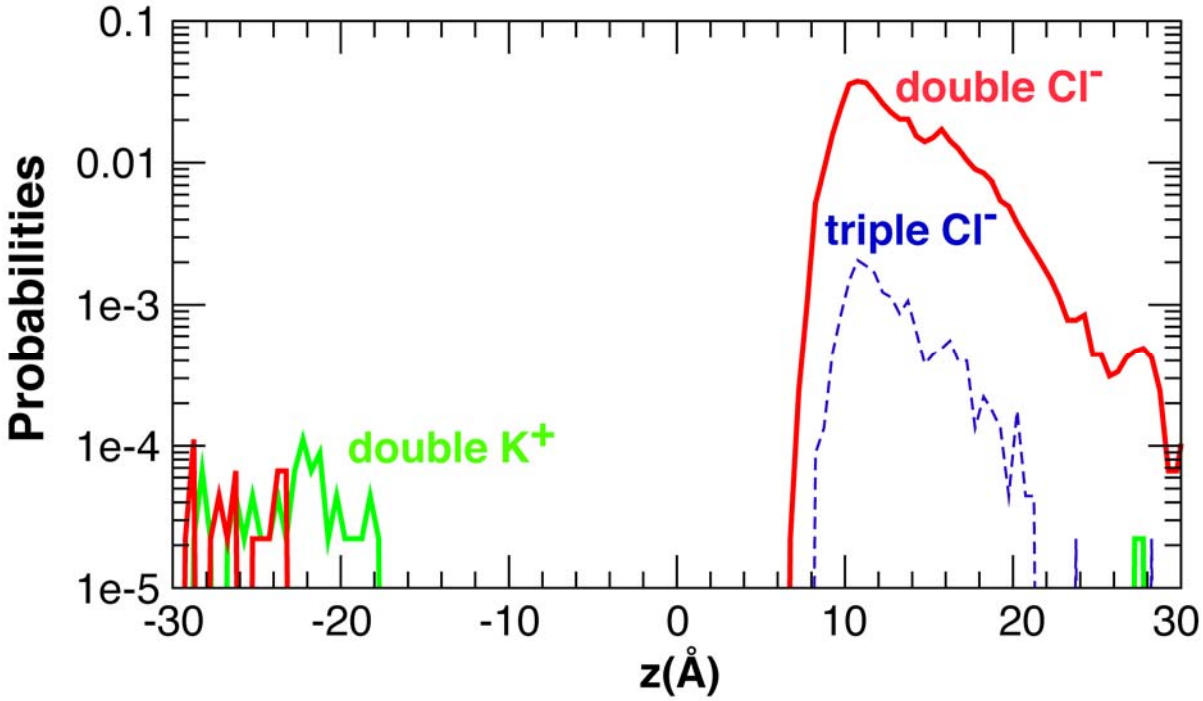

Figure 3. Probabilities of finding multiple ions within the 8 Å-radius cylinder centered at the pore center of mass as a function of the *z* displacement. These probabilities were derived from the 20-ns equilibrium simulation trajectory [28]. Two or more ions were considered to be occupying the same xy-plane if their separation along z-axis was no bigger than 0.5 Å. The probabilities of more than double K^+ or triple Cl^- occupancy were small and thus not shown.

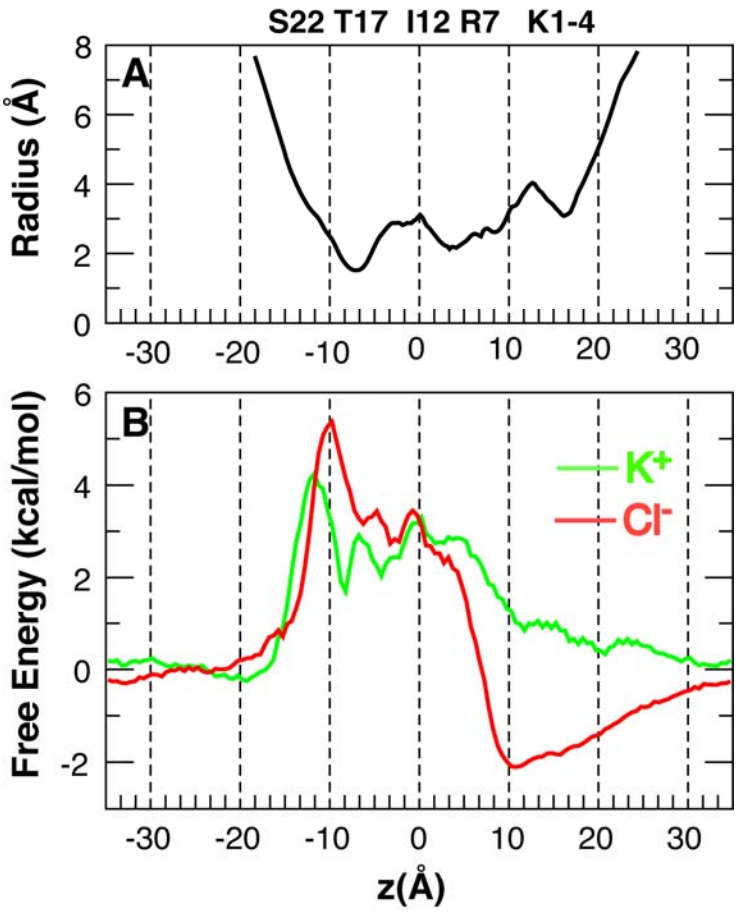

Figure 4. The pore radius and overall PMFs of K^+ and Cl^- permeation through the model p22 pentameric pore. Approximate locations of several key residues are marked. The overall PMFs were constructed by combining the results from umbrella sampling and equilibrium simulations using linear interpolation (see Methods). The pore radius profile was computed using HOLE [47].

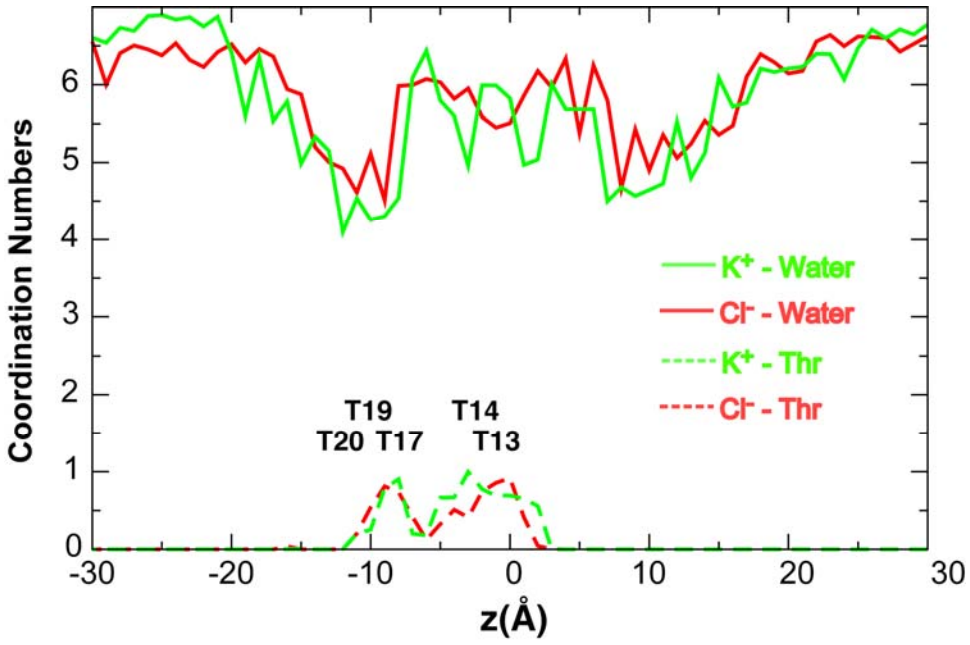

Figure 5. Average numbers of coordinating water molecules and threonine hydroxyls as a function of *z* displacement from the pore center of mass. The approximate locations of rings of threonine hydroxyls are also marked.

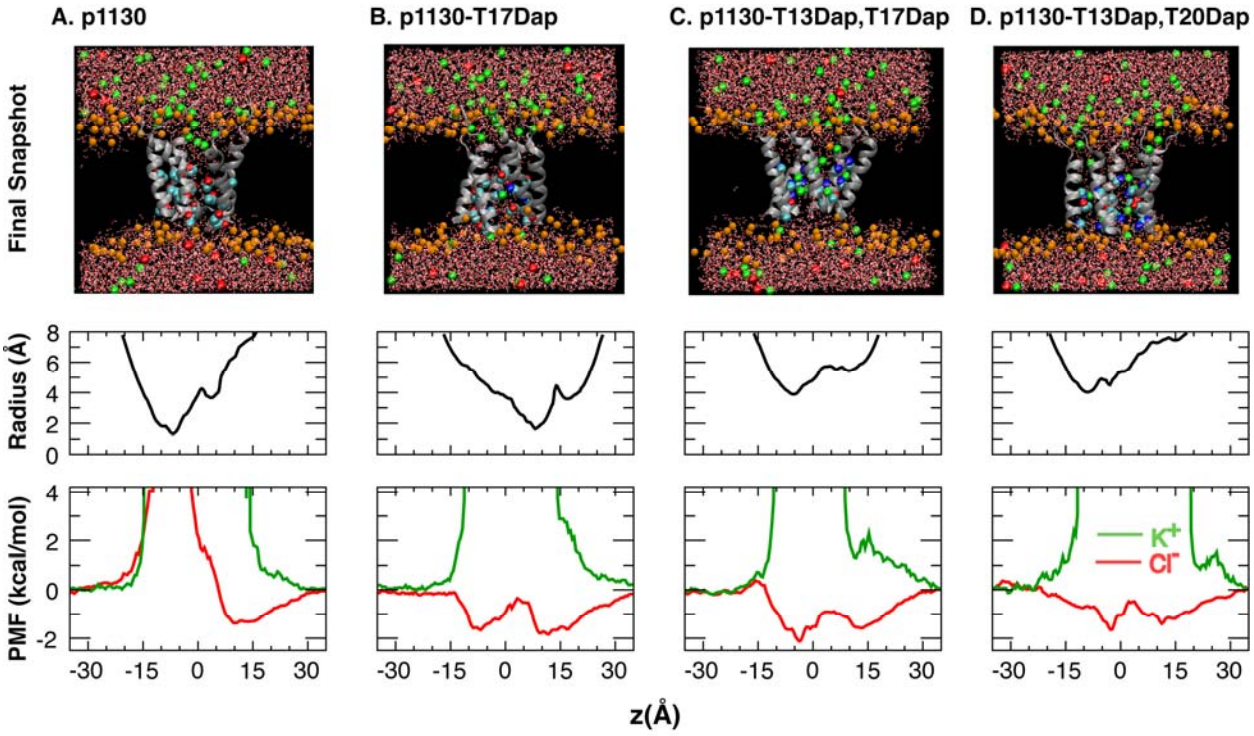

Figure 6. Summary of equilibrium simulations of p1130 and several singly and doubly Dap substituted sequences. The pore profiles (middle row) were computed using HOLE based on the last snapshots shown (top row). The PMFs (bottom row) were converted directly from the equilibrium ion densities. Note that regions with high free energies (e.g., > 3 kcal/mol) are not converged in equilibrium simulations. The lipid molecules are not shown in the snapshots for clarity. Green spheres represent Cl^- ions and yellow spheres represent phosphorus atoms of lipid head groups.